

Possible mechanism responsible for observed impurity outward flow under radio frequency heating

S. Moradi, T. Fülöp, A. Mollén, I. Pusztai

Department of Applied Physics, Nuclear Engineering, Chalmers University of Technology and Euratom-VR Association, Göteborg, Sweden

Abstract. The effect of poloidal asymmetry of impurities on impurity transport driven by electrostatic turbulence in tokamak plasmas is analyzed. It is found that in the presence of in-out asymmetric impurity populations the zero-flux impurity density gradient (the so-called peaking factor) is significantly reduced. A sign change in the impurity flux may occur if the asymmetry is sufficiently large. This may be a contributing reason for the observed outward convection of impurities in the presence of radio frequency heating. The effect of in-out asymmetry is most significant in regions with low temperature gradients. In the trapped electron mode dominated case also an up-down asymmetry can lead to a sign change in the peaking factor from positive to negative. The effect of ion parallel compressibility on the peaking factor is significant, and leads to positive peaking factors in regions with high temperature gradients, even in the presence of in-out asymmetry.

PACS numbers: 52.25 Fi, 52.25 Ya, 52.55 Fa

1. Introduction

Accumulation of impurities in the core of fusion devices would have detrimental effect on fusion reactivity due to increased radiation losses and plasma dilution. Significant effort has therefore been spent during recent years to identify plasma conditions in which accumulation can be avoided. One of the most promising methods for obtaining flat or hollow impurity density profiles is to use radio frequency heating. This has been shown to work well in various experiments [1, 2, 3, 4, 5, 6, 7] but the physical mechanism by which the change of the direction of the impurity convective velocity occurs has not yet been clearly identified in spite of the various efforts that have been made [8, 9, 10]. In particular the reason for the flat impurity density profiles in ion cyclotron resonance heated (ICRH) discharges in JET has been debated for many years [1, 5, 6]. In a recent paper [11] it was shown that a poloidal asymmetry could lead to a significant reduction of the impurity zero-flux density gradient (also called the peaking factor), and even a sign change in the impurity flux, if the asymmetry is sufficiently large. This suggests a possible explanation for the avoidance of accumulation of high- Z impurities with ICRH.

In this paper a numerical investigation of the effect of poloidal asymmetry on impurity transport is presented. In particular, the dependence of the impurity density peaking factor on charge number, inverse ion- and electron temperature scale lengths and inverse electron density scale length is analyzed. Also, the role of parallel ion compressibility is studied. The results are benchmarked to GYRO [12] in the poloidally symmetric case.

It is found that inboard accumulation gives rise to negative peaking factors (outward impurity convection and hollow impurity profile), both in ion temperature gradient (ITG) and trapped electron (TE) mode driven turbulence. The sign and magnitude of the peaking factor will be shown to be sensitive not only to the asymmetry strength but also to the temperature gradient, and it is more pronounced in the low temperature gradient region characteristic for the plasma core. The peaking factor is expected to be negative for moderate to high impurity charge numbers (above $Z \simeq 15$) for JET-like experimental parameters [1]. In TE mode dominated cases up-down asymmetry can also give rise to negative peaking factors if the electron temperature gradient is sufficiently large. As noted in previous work [8], in the poloidally symmetric case, that parallel compressibility has a significant effect on the peaking factor. As we will see in this paper this effect is even more pronounced for asymmetric impurity densities, and will lead to negative peaking factors for lower asymmetry strengths than without taking into account parallel compressibility.

The remainder of the paper is organized as follows. In Sec. 2 we describe the mechanism behind the impurity poloidal asymmetry that arises in the presence of ICRH. In Sec. 3 the model for calculating the quasilinear impurity flux and the peaking factor in the presence of poloidal asymmetry is presented. In Sec. 4 the parametric dependences of the peaking factor are analyzed by presenting scans over relevant parameters such as charge number, and temperature and density scale lengths. Also, the importance of the

impurity parallel compressibility is demonstrated. Finally, the results are discussed and summarized in Sec. 5.

2. Poloidal asymmetry

Poloidal impurity asymmetries in tokamaks can arise due to various reasons: e.g. difference in impurity source location, toroidal rotation or neoclassical effects. There is a wealth of experimental evidence for poloidal asymmetries [13, 14, 15, 16, 17, 18]. In the plasma core in-out asymmetries can arise due to the presence of radio frequency (RF) heating (henceforth “in-out” and “out-in” asymmetries will refer to the situations when the maximum of the poloidally varying impurity density is at the inboard and outboard sides of the plasma, respectively). A detailed physical explanation of why ICRH favors inboard accumulation, together with the description of the experimental results, is given in Ref. [13]. The underlying principle is that the asymmetry is a result of the increase of the hydrogen-minority density on the outboard side. These particles tend to be trapped on the outside of the torus and the turning points of their orbits drift towards the resonance layer due to the heating. The poloidal asymmetry in the hydrogen-minority density gives rise to an electric field that pushes the other ion species to the inboard side. In the case of highly-charged impurities, this effect is amplified by their higher charge Z .

The RF-induced accumulation of minority ions on the outboard side leads to a corresponding impurity accumulation on the inboard side by the following mechanism. If the plasma consists of electrons, bulk ions, impurity ions and RF-heated minority ions then it can be expected that all species except the minority ions are Boltzmann distributed (the dynamics of the minority ions is strongly affected by the heating). If a particle species a is Boltzmann distributed, the poloidal variation of the density is $\tilde{n}_a/n_{a0} \simeq -e_a\phi/T_a$, where the tilde denotes the variation on the flux surface, e_a is the charge and T_a is the temperature of the species. Quasineutrality requires that

$$n_{e0} \left(1 + \frac{e\phi}{T_e}\right) - n_{D0} \left(1 - \frac{e\phi}{T_i}\right) - Zn_{z0} \left(1 - \frac{Ze\phi}{T_z}\right) = n_{H0} + \tilde{n}_H,$$

where the subscript zero indicates the density where the potential ϕ vanishes. If ϕ is normalized so that $n_{D0} + n_{H0} + Zn_{z0} - n_{e0} = 0$, the poloidal variation of the impurity density becomes

$$\frac{\tilde{n}_z}{n_{z0}} = -\frac{Ze\phi}{T_z} = -\frac{Z\tilde{n}_H/n_{D0}}{1 + (T_i/T_e) + (n_{z0}Z^2/n_{D0})}. \quad (1)$$

Since the poloidal variation in the impurity density has the opposite sign to that of the minority ions, the accumulation of the latter on the outboard side gives rise to an electric field that pushes the other ion species to the inboard side. Simulations of the hydrogen ion distribution function in the presence of RF heating with the Monte Carlo code FIDO [19] show that a considerable out-in asymmetry in the hydrogen ion density

can be expected, which is sufficient to account for the observed in-out asymmetry in the impurity density.

In the tokamak edge, where the plasma is sufficiently collisional, also steep radial pressure or temperature gradients can give rise to an in-out asymmetry. These effects have been observed in e.g. Alcator C-Mod [14], and it has been shown that the observations are in qualitative agreement with neoclassical theory [20, 21, 22, 23]. The sign and magnitude of these asymmetries depend sensitively and nonlinearly on magnetic geometry, fraction of impurities in the plasma and rotation. Neoclassical theory also predicts an up-down asymmetry, which is caused by the ion-impurity friction.

3. Impurity flux

Since impurity transport is usually dominated by drift-wave turbulence, in this work we focus on the effect of the impurity poloidal asymmetry on impurity transport driven by microinstabilities. We assume that the processes that cause the asymmetry are not affected significantly by the fact that the cross-field transport is dominated by fluctuations. For simplicity we consider only the collisionless, electrostatic case. The quasilinear impurity particle flux is given by

$$\Gamma_z = -\frac{k_\theta}{B} \text{Im} [\hat{n}_z \phi^*], \quad (2)$$

where $\text{Im}[\cdot]$ denotes imaginary part, k_θ is the poloidal wave-number, \hat{n}_z is the perturbed impurity density, ϕ^* is the complex conjugate of perturbed electrostatic potential ϕ .

The perturbed impurity density response in an axisymmetric, large aspect ratio torus with circular magnetic surfaces can be obtained from the linearized gyrokinetic equation [24]. In the absence of collisions and in the limit $v_\parallel/qR(\omega - \omega_{Dz}) \ll 1$, the gyrokinetic equation can be solved iteratively to find the non-adiabatic part of the perturbed impurity distribution

$$g_z = \left(1 - \frac{v_\parallel}{qR(\omega - \omega_{Dz})} \frac{\partial}{\partial \theta} \frac{v_\parallel}{qR(\omega - \omega_{Dz})} \frac{\partial}{\partial \theta} \right) \frac{Z e f_{z0}}{T_z} \frac{\omega - \omega_{*z}^T}{\omega - \omega_{Dz}} J_0(z_z) \phi,$$

where θ is the extended poloidal angle, $f_{a0} = n_a / (\sqrt{\pi} v_{Ta})^3 \exp(-x_a^2)$ is the equilibrium Maxwellian distribution function, $x_a = v/v_{Ta}$ is the velocity normalized to the thermal speed $v_{Ta} = (2T_a/m_a)^{1/2}$, n_a and m_a are the density and mass of species a , $\omega_{*a} = -k_\theta T_a / e_a B L_{na}$ is the diamagnetic frequency, $\omega_{*a}^T = \omega_{*a} \left[1 + \left(x_a^2 - \frac{3}{2} \right) L_{na} / L_{Ta} \right]$, $L_{na} = -[\partial(\ln n_a) / \partial r]^{-1}$, $L_{Ta} = -[\partial(\ln T_a) / \partial r]^{-1}$, are the density and temperature scale lengths, $\omega_{Da} = -k_\theta (v_\perp^2 / 2 + v_\parallel^2) D(\theta) / \omega_{ca} R$ is the magnetic drift frequency, $D(\theta) = (\cos \theta + s \theta \sin \theta)$, $\omega_{ca} = e_a B / m_a$ is the cyclotron frequency, B is the equilibrium magnetic field, q is the safety factor, $s = (r/q)(dq/dr)$ is the magnetic shear, r and R are the minor and major radii, J_0 is the Bessel function of the first kind and $z_a = k_\perp v_\perp / \omega_{ca}$. Including the Boltzmann part of the distribution, the perturbed ion density response becomes [24, 25]

$$\frac{\hat{n}_z}{n_z} = -\frac{Z e \phi}{T_z} + \int d^3 v \frac{Z e f_{z0} J_0(z_z)}{n_z T_z} \left[1 - \frac{v_\parallel}{qR(\omega - \omega_{Dz})} \frac{\partial}{\partial \theta} \frac{v_\parallel}{qR(\omega - \omega_{Dz})} \frac{\partial}{\partial \theta} \right] \frac{\omega - \omega_{*z}^T}{\omega - \omega_{Dz}} J_0(z_z) \phi,$$

(3)

where parallel compressibility is represented by the term containing the two θ -derivatives.

The zero-flux impurity density gradient (the peaking factor) can be obtained from $\langle \Gamma_z \rangle = 0$ with the perturbed impurity density taken from (3). Here $\langle \dots \rangle = (1/2\pi) \int_{-\pi}^{\pi} (\dots) d\theta$. If the impurity density varies over the flux surface, in general we can write $n_z = n_{z0} \mathcal{P}(\theta)$, where $\mathcal{P}(\theta) = 1$ if the impurities are evenly distributed over the flux surface. A poloidal asymmetry can be modelled by $\mathcal{P}(\theta) = \left[\cos^2 \left(\frac{\theta - \delta}{2} \right) \right]^n$, where δ is the angular position where the impurity density has its maximum. This asymmetry function was used also in previous work [11, 15]. Figure 1 shows the asymmetry function $\mathcal{P}(\theta)$ as a function of normalized θ/π , for $n = 4$ and different values of δ .

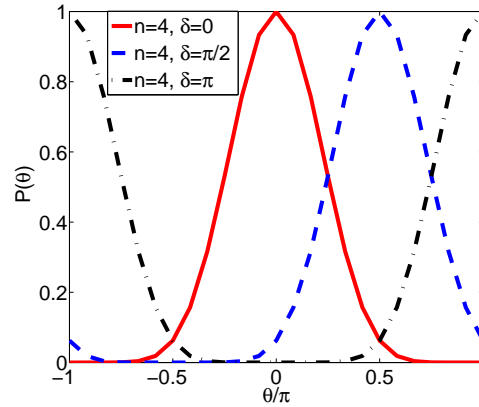


Figure 1. $\mathcal{P}(\theta)$ as a function of normalized θ/π , for different values of the peaking angle δ . The asymmetry strength is $n = 4$. Solid line (red) represents out-in, dashed line (blue) is up-down and dash-dotted line (black) is in-out asymmetry.

The impurity flux can be calculated numerically, by solving the velocity-space integrals in the perturbed impurity density (3) in the expression for the impurity flux (2), without the constant energy resonance approximation or the assumption on the smallness of the finite Larmor radius parameter. Then the impurity peaking factor a/L_{nz}^0 can be obtained by setting the impurity flux to zero, or $\langle \text{Im}[\hat{n}_z \phi^*] \rangle = 0$. Here, the fluctuating density is given by Eq. (3), a is the outermost minor radius, and a/L_{nz}^0 is calculated as

$$a/L_{nz}^0 = \frac{\langle \text{Im}[S_T(\theta) \phi^*] \rangle}{\langle \text{Im}[S_n(\theta) \phi^*] \rangle}, \quad (4)$$

where

$$S_n(\theta) = \int d^3 x_z e^{-x_z^2} J_0[z_z(\theta)] (1 - \delta_p \mathcal{M}_\theta) \frac{\bar{\omega}_{*z} \mathcal{P}(\theta) \phi(\theta) J_0[z_z(\theta)]}{\bar{\omega} - \bar{\omega}_{Dz}(\theta)}, \quad (5)$$

and

$$S_T(\theta) = \int d^3 x_z e^{-x_z^2} J_0[z_z(\theta)] (1 - \delta_p \mathcal{M}_\theta) \frac{[\bar{\omega} - \bar{\omega}_{*z}(x_z^2 - 3/2)a/L_{Tz}] \mathcal{P}(\theta) \phi(\theta) J_0[z_z(\theta)]}{\bar{\omega} - \bar{\omega}_{Dz}(\theta)}, \quad (6)$$

with the operator representing parallel compressibility

$$\mathcal{M}_\theta = \frac{x_{z\parallel}}{R(\theta)(\bar{\omega} - \bar{\omega}_{Dz}(\theta))} \frac{\partial}{\partial \theta} \frac{x_{z\parallel}}{R(\theta)(\bar{\omega} - \bar{\omega}_{Dz}(\theta))} \frac{\partial}{\partial \theta}, \quad (7)$$

where $R(\theta) = R_0(1 + \epsilon \cos \theta)$ with $\epsilon = r/R_0$, $\delta_p = 2a^2 m_i / (q^2 m_z \tau_z)$, $\tau_z = T_e / T_z$, $b = (\rho_s / Z) \sqrt{2A_Z / \tau_z A_i}$, ρ_s is the ion sound Larmor radius, $\bar{\omega}_{*z} = -k_\theta \rho_s / Z \tau_z$, $\bar{\omega}_{Dz} = -2k_\theta \rho_s (a/R)(x_{z\perp}^2 / 2 + x_{z\parallel}^2) D(\theta) / Z \tau_z$, $z_z(\theta) = x_{z\perp} b k_\perp(\theta)$, and $k_\perp = k_\theta \sqrt{1 + s^2 \theta^2}$. All frequencies marked with bars are in c_s/a units, where c_s is the ion sound speed, and the main ion and impurity temperature gradients are assumed to be equal $a/L_{Tz} = a/L_{Ti}$.

4. Parametric dependences of the peaking factor

In the calculations presented in this section we have used the following local profile and magnetic geometry parameters: $r/a = 0.3$, $R/a = 3$, $k_\theta \rho_s = 0.3$, $q = 1.7$, $a/L_{ne} = 1.3$, $a/L_{ni} = 0.86$, $T_i/T_e = 0.85$, $a/L_{Te} = 0.2$, $a/L_{Ti} = 0.3$, $s = 0.22$ and $\rho_s/a = 0.0035$. These parameters have been taken from a typical JET-shot with ICRH [1]. The impurities are assumed to be present in trace quantities, in the sense that $Zn_z/n_e \ll 1$ ($n_z/n_e = 10^{-3}$ is used in the simulations). This is the baseline case in our study, and these parameters will be used unless otherwise stated. The perturbed electrostatic potential and eigenvalues have been obtained by linear electrostatic gyrokinetic calculations with GYRO.

4.1. Charge number dependence

The peaking factor as a function of charge number for various impurity poloidal asymmetries is shown in Fig. 2. In the poloidally symmetric case (solid line in Fig. 2a), the peaking factor is not sensitive to the charge number, as has been noted before, in both fluid and gyrokinetic simulations of ITG turbulence dominated transport, without taking into account the poloidal impurity asymmetries [8, 26]. The situation is similar also in case of up-down asymmetric impurity populations, while the peaking factor increases slightly in case of outboard accumulation. However, in agreement with the conclusion of [11], the black dotted line in Fig. 2a shows that impurities experience outward convection (corresponding to negative peaking factor) if the impurity density is accumulated on the inboard side. The change in the peaking factor becomes stronger as the asymmetry is increased, as it is illustrated in Fig. 2b. Note, that the strength of the asymmetry is also expected to depend on Z , and usually it is larger for heavy impurities, as it was shown in Sec. 2. According to Eq. (1), in the limit of trace impurities, the poloidal variation of the impurity density is proportional to the charge number.

In order to examine the importance of parallel compressibility in determining the charge dependence of the impurity peaking factor we separate the terms independent and proportional to δ_p (representing the parallel compressibility) in Eq. (5) as $S_n(\theta) = S_n^1(\theta) + S_n^{pc}(\theta)$, where

$$S_n^1(\theta) = \mathcal{P}(\theta) \phi(\theta) \int d^3 x_z e^{-x_z^2} J_0^2[z_z(\theta)] \frac{\bar{\omega}_{*z}}{\bar{\omega} - \bar{\omega}_{Dz}(\theta)}, \quad (8)$$

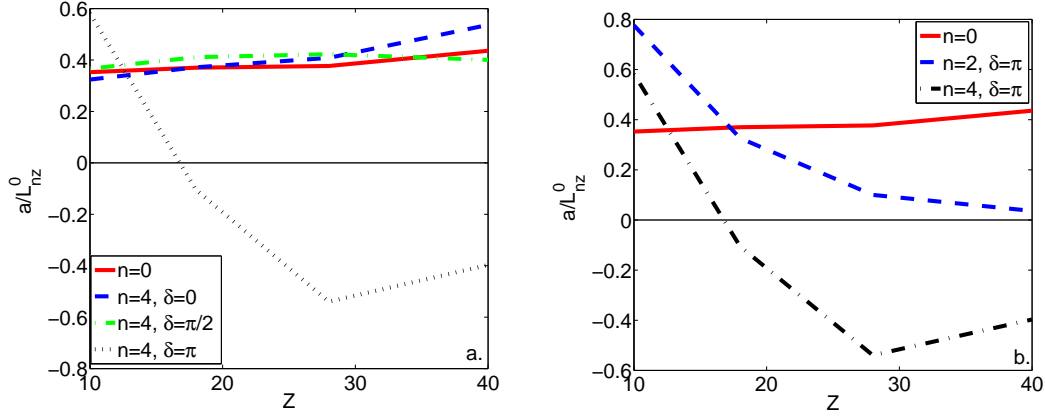


Figure 2. Peaking factor as a function of charge number for different values of peaking angle δ (a) and asymmetry strength n (b). The rest of the parameters are taken from the baseline case, for which the eigenvalue is $\omega = (0.001 + i 0.068)c_s/a$. In both figures the solid line represents the case of poloidally symmetric impurity distribution. (a): $n = 4$ – out-in asymmetry (dashed), up-down asymmetry (dash-dotted), in-out asymmetry (dotted). (b): in-out asymmetry – $n = 2$ (dashed), $n = 4$ (dash-dotted).

$$S_n^{pc}(\theta) = -\delta_p \int d^3x_z e^{-x_z^2} J_0[z_z(\theta)] \mathcal{M}_\theta \frac{\bar{\omega}_{*z} \mathcal{P}(\theta) \phi(\theta) J_0[z_z(\theta)]}{\bar{\omega} - \bar{\omega}_{Dz}(\theta)}, \quad (9)$$

and in Eq. (6) as $S_T(\theta) = S_T^1(\theta) + S_T^{pc}(\theta)$, where

$$S_T^1(\theta) = \mathcal{P}(\theta) \phi(\theta) \int d^3x_z e^{-x_z^2} J_0^2[z_z(\theta)] \frac{\bar{\omega} - \bar{\omega}_{*z}(x_z^2 - 3/2)a/L_{Tz}}{\bar{\omega} - \bar{\omega}_{Dz}(\theta)}, \quad (10)$$

$$S_T^{pc}(\theta) = -\delta_p \int d^3x_z e^{-x_z^2} J_0[z_z(\theta)] \mathcal{M}_\theta \frac{[\bar{\omega} - \bar{\omega}_{*z}(x_z^2 - 3/2)a/L_{Tz}] \mathcal{P}(\theta) \phi(\theta) J_0[z_z(\theta)]}{\bar{\omega} - \bar{\omega}_{Dz}(\theta)}. \quad (11)$$

Using the above notations the peaking factor can be rewritten as:

$$a/L_{nz}^0 = \frac{\langle \text{Im}[S_T^1(\theta) \phi^*] \rangle + \langle \text{Im}[S_T^{pc}(\theta) \phi^*] \rangle}{\langle \text{Im}[S_n^1(\theta) \phi^*] \rangle + \langle \text{Im}[S_n^{pc}(\theta) \phi^*] \rangle}. \quad (12)$$

Figure 3 shows these four expressions as functions of impurity charge for the symmetric and in-out asymmetric cases with an asymmetry strength of $n = 4$. In the denominator, the terms independent of δ_p , i.e. $S_n^1(\theta)$, are the dominant contributors in both the symmetric and asymmetric cases. These are proportional to $1/Z$. But in the numerator, the balance between the terms proportional and independent of δ_p is very different between the symmetric and asymmetric cases; in the symmetric case $S_T^1(\theta)$ is the dominant term, while in the asymmetric case $S_T^{pc}(\theta)$ is dominant. This latter term, which is due to parallel compressibility, changes sign at moderate charge numbers ($Z \simeq 15$), which in turn leads to a sign-change in the peaking factor. These results show that if an in-out asymmetry is present, the parallel compressibility effects become more important than the other terms, and therefore, have to be taken into account.

In the following we will concentrate on the peaking factor for nickel which was one of the impurities studied in Ref. [1]. Figure 4 shows the peaking factor for nickel

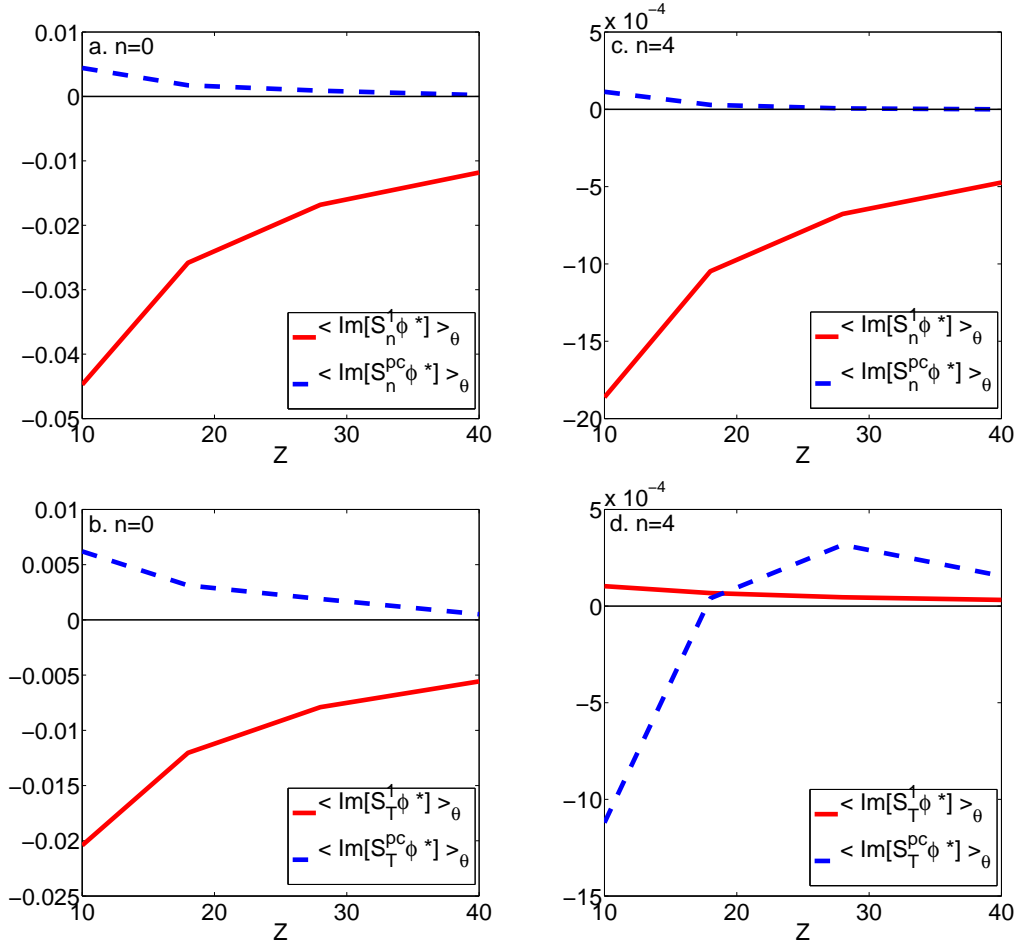


Figure 3. Terms proportional (dashed lines) and independent of δ_p (solid lines) in Eq. (12) as functions of impurity charge Z . (a) and (c) show the terms in the denominator and (b) and (d) show the terms in the numerator. (a) and (b) correspond to the poloidally symmetric case, and (c) and (d) correspond to in-out asymmetry with strength $n = 4$.

for various accumulation maxima δ and asymmetry strengths n . The peaking factor increases slightly for up-down accumulation but the more dramatic change – including a sign-change – is expected only for inboard accumulation. The sign change occurs when $n \simeq 2$. In Ref. [11] it was shown that without taking into account the effect of parallel compressibility the sign change occurs when $n \simeq 3$. This is in agreement with the results obtained here when parallel compressibility effects are neglected, i.e. by setting $\delta_p = 0$ in Eqs. (5) and (6) (as will be shown later in Fig. 13).

Assuming that by increasing the RF heating and therefore the temperature gradients, the asymmetry will increase as well, e.g. $n \propto a/L_T$ the results shown in Fig. 4a can be linked to the experimental results illustrated in Figs. 6 and 7 in Ref. [1]. In this reference the experimental observation of the effect of ICRH heating on the nickel transport in the plasma core at JET is discussed. It is shown that the application of

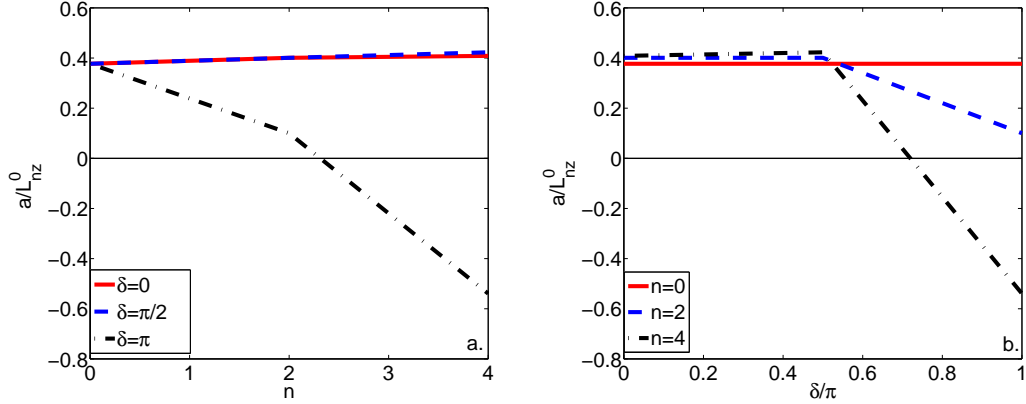


Figure 4. Peaking factor for nickel as a function of n (a) and δ (b). (a): symmetric impurity density (solid, red), up-down asymmetry (dashed, blue), and in-out asymmetry (dash-dotted, black). (b): symmetric impurity density (solid, red), $n = 2$ (dashed, blue), $n = 4$ (dash-dotted, black).

the ICRH leads to an outward impurity flux (negative peaking factor). As the applied heating is increased and therefore, the temperature gradient peaked, the outward flux is further increased leading to more negative peaking factors.

4.2. Temperature gradient dependence

The eigenvalues and electrostatic potentials as functions of ion- and electron temperature gradients are shown in Figs. 5-6. As expected, if we increase the ion temperature

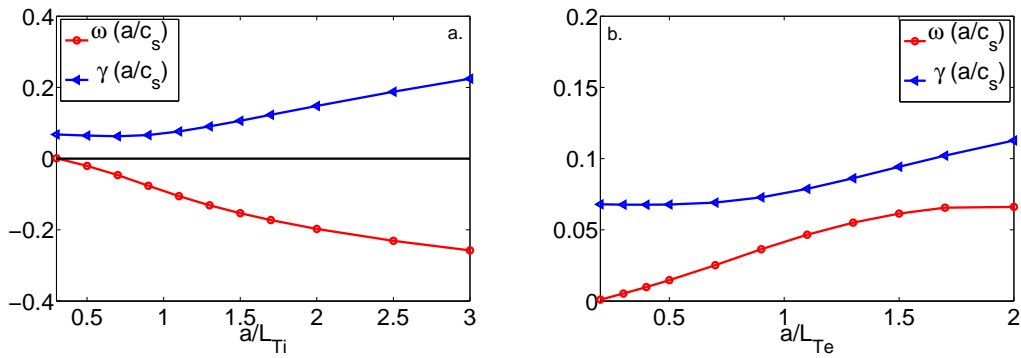


Figure 5. Real and imaginary parts of $\omega = \omega_r + i\gamma$ as function of a/L_{Ti} (a) and a/L_{Te} (b) obtained by GYRO for the baseline case. Blue lines (with circle markers) represent the real part, blue lines (triangle markers) correspond to the imaginary part of the eigenvalue. The frequencies are normalized to c_s/a .

gradient, the turbulence becomes more ITG-dominated (the real part of the mode frequency ω_r is negative), while if we increase the electron temperature gradient, TE-mode driven turbulence will dominate (ω_r is positive). The shape of the imaginary

part of the potential $\text{Im}[\phi]$ varies strongly by increasing the temperature gradient for both the ITG and TE-mode dominated cases, while the real parts of the potential $\text{Re}[\phi]$ are not modified significantly, see Fig. 6. The imaginary part of the potential plays

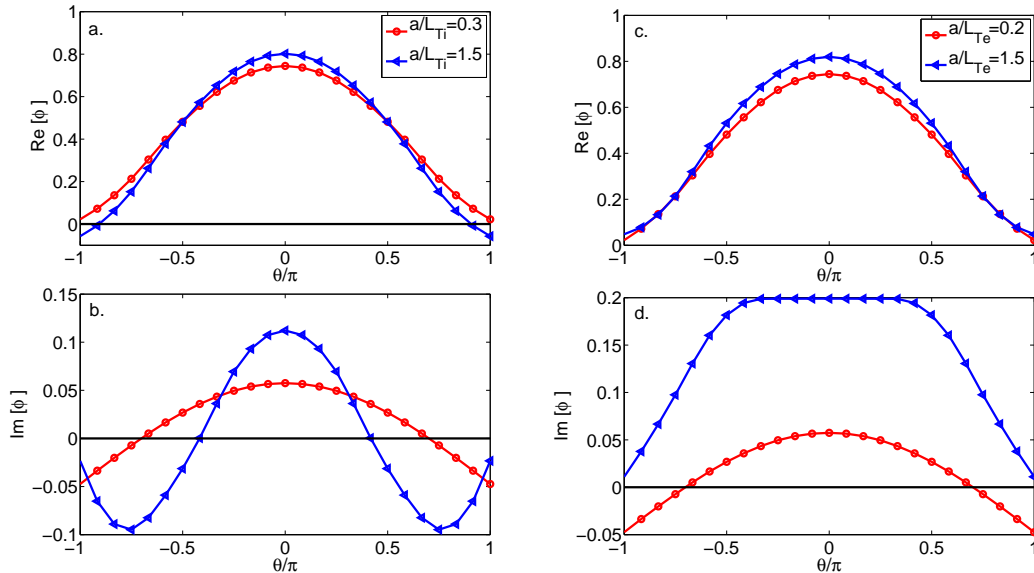


Figure 6. Real and imaginary parts of the electrostatic potentials in the cases corresponding to Fig. 5 for different ion- (a,b) and electron (c,d) temperature gradients. (a) and (c) show the real parts and (b) and (d) show the imaginary parts of ϕ (note the different scale). Red lines (circle markers) show the temperature gradient corresponding to the baseline case and blue lines (triangle markers) show the case with the larger temperature gradient.

an important role in the parallel compressibility terms and therefore the change in the temperature gradient will modify the impurity peaking factor considerably.

Previous works highlighted the difference in peaking factors in ITG and TE dominated cases, and concluded that ITG-dominated turbulence will always generate inward pinch of impurities, while in TE-mode driven turbulence outward convection in the plasma core (for $r/a \simeq 0.2$) can be expected. Both linear [7, 8] and non-linear [27] gyrokinetic simulations have shown that the latter is due to the contribution from the parallel dynamics which can reverse the impurity convection from inwards to outwards for modes propagating in the electron direction. These results are in agreement, under some conditions, with the experimental observation that the impurity convection changes sign from inward to outward when a strong central peaking of the electron temperature arises as a response to strong localized central electron heating. However, these results cannot explain the outward convection of impurities observed in experiments with RF heating where the ITG-mode is the dominant instability.

Our results show, that the peaking factor is negative in both ITG- and TE-dominated cases if the impurities accumulate on the inboard side. However, the peaking

factor is influenced very strongly by increasing temperature gradients and will become positive again above a certain temperature gradient.

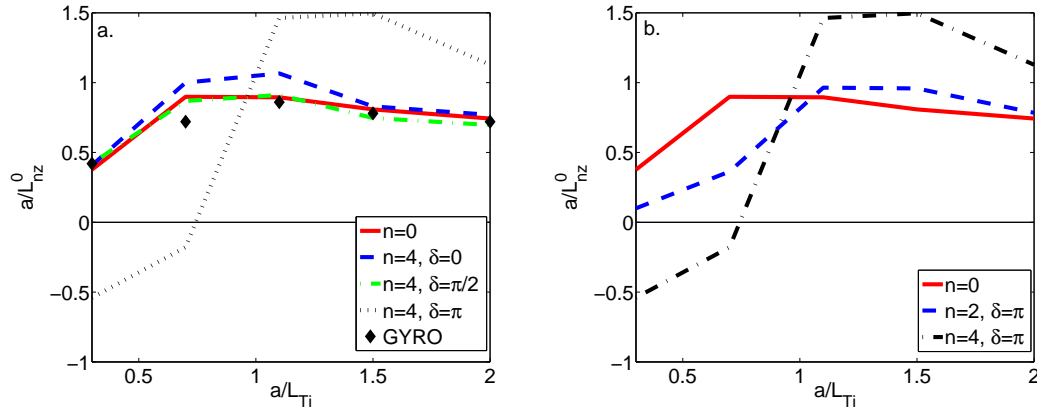


Figure 7. Peaking factor for nickel as a function of ion temperature gradient for different values of δ (a) and n (b). In both figures the solid line represents the case of poloidally symmetric impurity distribution; in figure (a) this case is compared to GYRO simulations (black diamonds). (a): $n = 4$ – out-in asymmetry (dashed), up-down asymmetry (dash-dotted), in-out asymmetry (dotted). (b): in-out asymmetry – $n = 2$ (dashed), $n = 4$ (dash-dotted).

Figure 7 shows the ion temperature-gradient scaling of the peaking factor and the diamond symbols show these values obtained by GYRO simulations in the poloidally symmetric limit, which present good agreement with our results. The peaking factor is not very sensitive to the ion temperature gradient as long as the impurity density is poloidally symmetric or if it is up-down or out-in asymmetric. However, if the impurity density is in-out asymmetric then the sign of the peaking factor is negative for low temperature gradients and positive (and even larger than in the poloidally symmetric case) for large temperature gradients. The threshold for the sign change for the experimental scenario studied in this paper is $a/L_{Ti} \simeq 1$. As the strength of the asymmetry, n , is increased for an in-out asymmetry the modifications of the peaking factor becomes stronger, see Fig. 7b.

As the electron temperature gradient is increased the turbulence becomes more TE dominated. Figure 8 shows that the absolute value of the peaking factor is reduced up to a certain temperature gradient and then starts to increase again, regardless of the sign of the asymmetry. The inboard accumulation gives negative peaking factors also in this case. One of the most interesting differences compared to the ITG-dominated case is that also an up-down asymmetry can lead to a sign change for $a/L_{Te} \simeq 0.5$. This can be a contributing reason for the observed flat impurity density profiles in plasmas with electron cyclotron resonance heating (ECRH), where the in-out accumulation mechanism described in [13] and in Sec. 2 would not be present. Up-down asymmetries have been observed in electron cyclotron (EC) heated plasmas [15]. The physical mechanism for these up-down asymmetries was attributed to neoclassical effects, but

since the magnitude of the asymmetries reported in Ref. [15] was very large it is possible that there are other reasons that may be related to the ECRH as well.

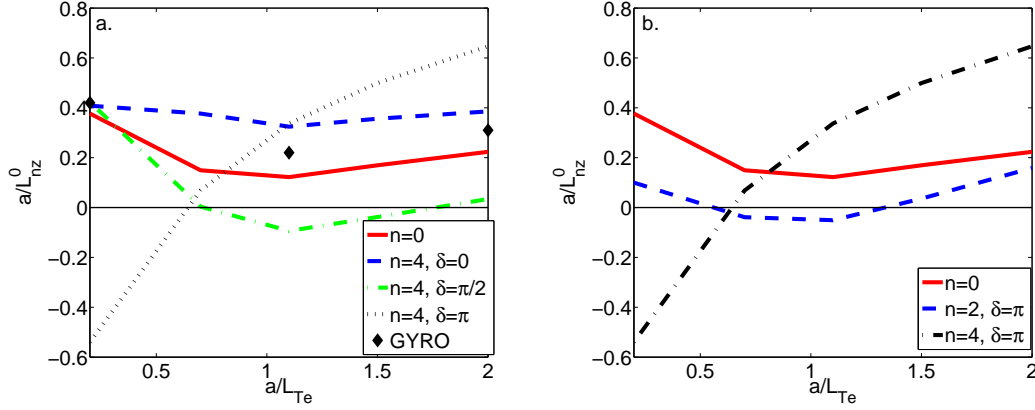


Figure 8. Peaking factor for nickel as a function of electron temperature gradient for different values of δ (a) and n (b). In both figures the solid line represents the case of poloidally symmetric impurity distribution; in figure (a) this case is compared to GYRO simulations (black diamonds). (a): $n = 4$ – out-in asymmetry (dashed, blue), up-down asymmetry (dash-dotted, green), in-out asymmetry (dotted, black). (b): in-out asymmetry – $n = 2$ (dashed, blue), $n = 4$ (dash-dotted, black).

4.3. Density gradient dependence

The density gradient scaling of the peaking factor is shown in Fig. 9. The peaking factor is slightly increasing in the case of poloidal symmetry and in the cases of up-down or out-in asymmetries, as the electron density peaking is increased. Also here, the in-out asymmetric impurity density leads to negative peaking factor if the strength of the asymmetry is sufficient. The peaking factor is fairly insensitive to the density gradient in this case. It is interesting to note, that even though the ITG-mode is the dominant instability here, (see Fig. 10), the peaking factor remains negative as the ITG-mode is becoming stronger in the case of an in-out asymmetry. This can be contrasted to the case when the stronger ion-temperature gradient led to a sign change and positive peaking factor, see Fig. 7a. The difference between the two cases can be understood by comparing the shape of the imaginary part of the electrostatic potential $\text{Im}[\phi]$ in Fig. 11b with that in Fig. 6b. It can be noted that by changing the temperature gradient, $\text{Im}[\phi]$ changes significantly, while changing the density profile does not result in a significant difference. Note that it is mainly the part of the potential which is close to $\theta = \pi$ which is important, and that is considerably different for the two temperature gradients shown in Fig. 6b and therefore also the result for the peaking factor changes dramatically. The difference in the electrostatic potentials is the underlying reason for the difference in the trends seen in Figs. 7 and 9 as the ITG-mode become stronger by increasing the a/L_{Ti} or a/L_{ne} , respectively.

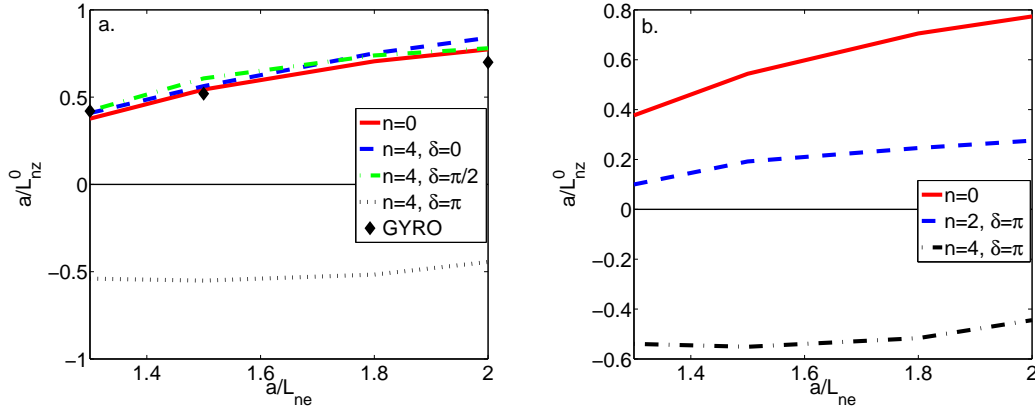


Figure 9. Peaking factor for nickel as a function of electron density gradient for different values of δ (a) and n (b). In both figures the solid line represents the case of poloidally symmetric impurity distribution; in figure (a) this case is compared to GYRO simulations (black diamonds). (a): $n = 4$ – out-in asymmetry (dashed, blue), up-down asymmetry (dash-dotted, green), in-out asymmetry (dotted, black). (b): in-out asymmetry – $n = 2$ (dashed, blue), $n = 4$ (dash-dotted, black).

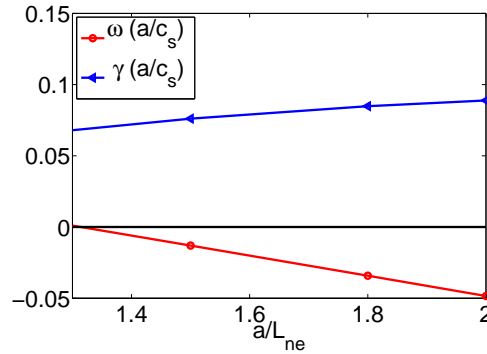


Figure 10. Real and imaginary parts of the eigenvalues as function of a/L_{ne} obtained by GYRO. Red lines (with circle markers) represent the real part, blue lines (triangle markers) correspond to the imaginary part of the eigenvalue. The frequencies are normalized to c_s/a .

4.4. Effect of parallel compressibility

It has been shown previously that when the transport is TE-mode dominated parallel compressibility effects generate an outward contribution to impurity anomalous flux which can, under certain plasma conditions, cancel out the inward contributions, leading to zero or even negative impurity peaking factor [7, 8]. In this subsection, we examine this effect by neglecting the parallel compressibility terms, i.e. terms proportional to δ_p in Eqs. (5) and (6). Note that in this case only the absolute value of the potential enters in the expressions, while in the case with parallel compressibility both the imaginary and real parts and their derivatives are important. Figure 12 illustrates the square of

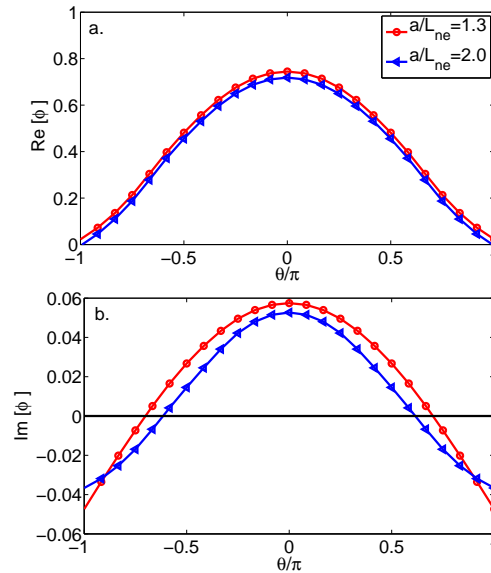


Figure 11. Real- (a) and imaginary (b) parts of the electrostatic potentials for two different density gradients.

the electrostatic potential $|\phi|^2$ for different values of a/L_{Ti} and a/L_{ne} . We note that

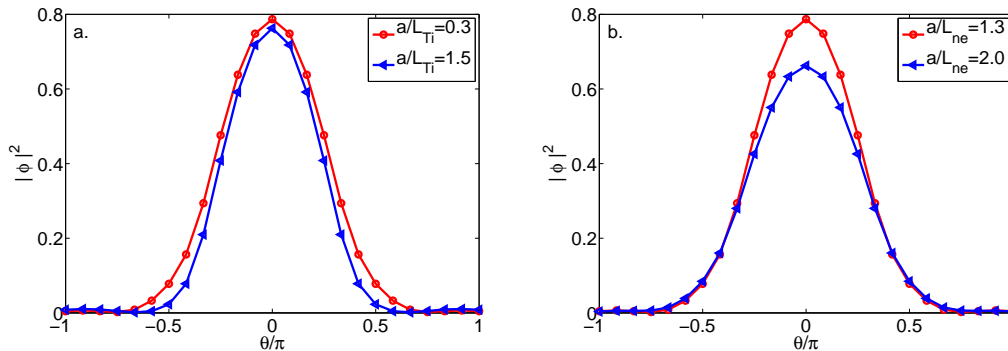


Figure 12. The square of the absolute value of the electrostatic potentials, $|\phi|^2$ for different ion temperature gradients and density gradients.

the absolute value of the potential is not significantly different in the various cases, so therefore we do not expect dramatic dependence on the temperature and density gradients. Figure 13 shows the peaking factor for various δ and n . The effect of poloidal asymmetry in this limit is in agreement with our previous work in Ref. [11] and also, is similar to that in the previous sections where the parallel compressibility effects are considered. As seen in Fig. 13a, in the absence of parallel compressibility effects an in-out asymmetry will lead to a negative peaking factor (outward impurity flux). An increase of the poloidal in-out asymmetry will increase the outward flux of impurities as shown in Fig. 13b. Note that in the case with parallel compressibility, the sign

change in the peaking factor occurs for broader range of δ and for lower asymmetry strength (compare Figs. 4 and 13). Also an up-down asymmetry can lead to a slight reduction of the impurity peaking factor. This is different from the case where the parallel compressibility was taken into account, see Fig. 4a.

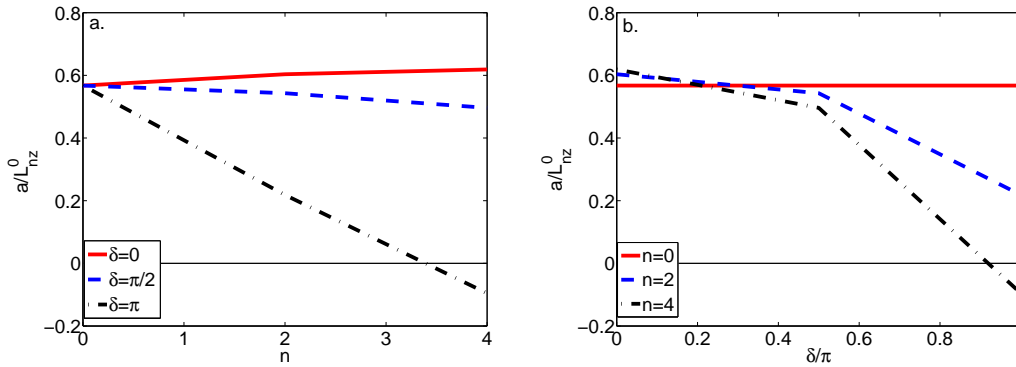


Figure 13. Peaking factor for nickel as a function of n (a) and δ (b), without taking into account parallel compressibility. (a): symmetric impurity density (solid, red), up-down asymmetry (dashed, blue), and in-out asymmetry (dash-dotted, black). (b): in-out asymmetry – symmetric impurity density (solid, red), $n = 2$ (dashed, blue), $n = 4$ (dash-dotted, black).

Figure 14 shows the density- and temperature-gradient and charge number scans for the peaking factor without parallel compressibility. The diamonds represent the values of peaking factor obtained by GYRO (without parallel compressibility) which show agreement with our results in the symmetric limit. From Fig. 14 it is clear that without parallel compressibility the effect of a poloidal asymmetry is almost insensitive to the increase of the gradients of temperatures and density or the impurity charge. This is mainly due to the fact that without parallel compressibility only the absolute value of the potential matters and that is rather similar in the various cases.

5. Discussion and conclusions

For tokamak operation the avoidance of central impurity accumulation is a key issue. Conditions in which the convective impurity flux is directed outward are particularly interesting. In order to find such conditions many experiments have been devoted to explore various techniques. One way to expel the impurities from the plasma core is to maintain sawtooth crashes in a controlled way by applying central ICRH [28, 29]. It is observed that this method will indeed remove the impurities from the plasma core. However, it was shown that even though sawtooth crashes hamper the accumulation of the impurities their contribution is less relevant compared to the effect of the ICRH itself [5]. Another technique which has been successful in removing the impurities from the plasma core and is routinely used in tokamak experiments such as in the ASDEX-U tokamak is the application of a very localized central ECRH [30]. Simulations with

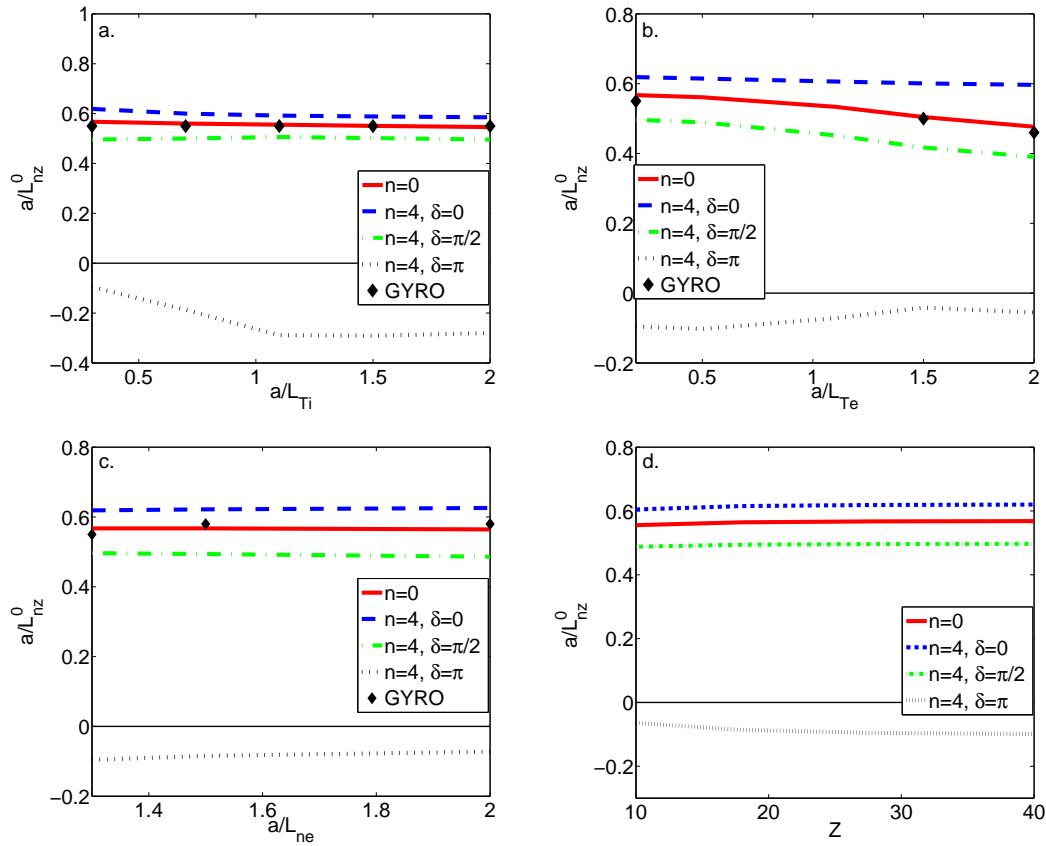


Figure 14. Peaking factor for nickel as a function of ion temperature gradient (a), electron temperature gradient (b) electron density gradient (c) and impurity charge Z (d) for different values of δ , without taking into account parallel compressibility. Solid (red) line represents the case of poloidally symmetric impurity distribution; in figures (a-c) this is compared to GYRO simulations (black diamonds). Out-in asymmetry (dashed, blue) up-down asymmetry (dash-dotted, green), in-out asymmetry (dotted, black).

both linear and non-linear gyrokinetic models have shown that under these conditions the electron temperature gradient is strongly peaked and therefore, modes propagating in the electron diamagnetic drift direction are the dominant instability responsible for the turbulence driven transport [27]. The interaction between the related electrostatic potential fluctuations and the parallel dynamics of the impurities leads to an outward convection of impurities. These results are in agreement with experimental observation in ASDEX-U for the very central region ($r/a \simeq 0.2$) [7]. In other tokamak experiments for example at JET the application of the central RF heating has also been explored with success. In these experiments it has been observed that the dominant instabilities are not TE-modes but rather modes directed in the ion diamagnetic drift direction, ITG-modes, which theoretically should result in an inward impurity flux. It has been debated that in the very central region of plasmas at JET the transport is mostly driven by neoclassical effects and by applying a strong central heating as the temperature gradient peaks the

neoclassical temperature screening effects become dominant and result in an outward directed impurity flux. Under some plasma conditions these effects may be the reason for the observed behavior [2] however, usually the observed transport is an order of magnitude larger than the neoclassical predictions implying that the impurity transport is turbulence driven [27].

In the present work we assume that the impurity density is in the form of $n_z(\theta) = n_{z0}\mathcal{P}(\theta)$ where the poloidal dependence is represented by $\mathcal{P}(\theta) = \left[\cos^2\left(\frac{\theta-\delta}{2}\right)\right]^n$, and discuss the impact of such a dependence on the impurity peaking factor in the core of tokamak plasmas. Various mechanisms may give rise to a poloidal asymmetry of impurity density: difference in impurity source location, toroidal rotation or neoclassical effects. Among these is an in-out poloidal asymmetry observed in plasmas where RF heating is applied. The mechanism responsible for this behavior was explained through RF-induced accumulation of minority ions on the outboard side of the torus giving rise to a corresponding impurity accumulation on the inboard side as was discussed in Sec. 2. The strength of the impurity accumulation depends on the impurity charge (higher for heavier impurities) and the plasma parameters such as temperature gradient. However, the exact form of these dependences is not yet known and further analysis is needed in this area.

We have found that an in-out poloidal asymmetry of the impurity density ($\delta = \pi$) can lead to an outward impurity flux (negative peaking factor) in both ITG and TE mode dominated cases, and this effect becomes stronger as the asymmetry strength (n) increases. In this case the peaking factor is strongly charge dependent and it becomes more negative for heavier impurities. In TE mode dominated case an up-down asymmetry can also generate a negative peaking factor. This can be a contributing reason for the observed flat impurity density profiles in plasmas with ECRH, and up-down asymmetries have indeed been observed in EC heated plasmas [15], although the physical mechanism for these asymmetries is not entirely understood.

The reason for the sign change of the impurity peaking factor in the presence of a poloidal asymmetry is attributed to the interaction between the poloidal variation of the related electrostatic potential and the poloidal dependence of the impurity density. If parallel compressibility effects are taken into account the imaginary part of the electrostatic potential is the determining factor in the sign change of the impurity peaking factor.

In summary, our results suggest that poloidal asymmetries can significantly alter the turbulence driven impurity transport and therefore, have to be taken into account. These asymmetries may have a significant role in determining the impurity accumulation properties in plasmas with radio frequency heating. Therefore, there is a strong need for development of new tools in order to detect poloidal asymmetries and determine the effect of RF heating in their generation and the dependence of the asymmetry function to various plasma parameters.

Acknowledgments

The authors would like to thank J Candy for providing the GYRO code. This work was funded by the European Communities under Association Contract between EURATOM and *Vetenskapsrådet*. The views and opinions expressed herein do not necessarily reflect those of the European Commission.

Reference

- [1] M. Valisa, L. Carraro, I. Predebon, M.E. Puiatti, C. Angioni, I. Coffey, C. Giroud, L. Lauro Taroni, B. Alper, M. Baruzzo, P. Belo daSilva, P. Buratti, L. Garzotti, D. Van Eester, E. Lerche, P. Mantica, V. Naulin, T. Tala, M. Tsalas and JET-EFDA contributors, *Nucl. Fusion*, **51** 033002 (2011).
- [2] R. Dux, R. Neu, A. G. Peeters, G. Pereverzev, A. Muck, F. Ryter, J. Stober and ASDEX Upgrade Team, *Plasma Phys. Control. Fusion*, **45** 1815 (2003).
- [3] R. Dux, C. Giroud, R. Neu, A.G. Peeters, J. Stober, K.-D. Zastrow, Contributors to the EFDA-JET Workprogramme, ASDEX Upgrade Team, *Journal of Nucl. Materials*, **313-316** 1150 (2003).
- [4] R. Neu, R. Dux, A. Geier, H. Greuner, K. Krieger, H. Maier, R. Pugno, V. Rohde, S.W. Yoon, ASDEX Upgrade Team, *Journal of Nucl. Materials*, **313-316**, 116 (2006).
- [5] M. E. Puiatti, M. Valisa, M. Mattioli, T. Bolzonella, A. Bortolon, I. Coffey, R. Dux, M. von Hellermann, P. Monier-Garbet, M. F. F. Nave, J. Ongena and contributors to the EFDA-JET Workprogramme, *Plasma Phys. Control. Fusion*, **45** 2011 (2003).
- [6] M. E. Puiatti, M. Valisa, C. Angioni, L. Garzotti, P. Mantica, M. Mattioli, L. Carraro, I. Coffey, C. Sozzi and JET-EFDA contributors, *Phys. Plasmas*, **13** 042501 (2006).
- [7] C. Angioni, L. Carraro, T. Dannert, N. Dubuit, R. Dux, C. Fuchs, X. Garbet, L. Garzotti, C. Giroud, R. Guirlet, F. Jenko, O. J. W. F. Kardaun, L. Lauro-Taroni, P. Mantica, M. Maslov, V. Naulin, R. Neu, A. G. Peeters, G. Pereverzev, M. E. Puiatti, T. Pütterich, J. Stober, M. Valovic, M. Valisa, H. Weisen, A. Zabolotsky, ASDEX Upgrade Team, and JET EFDA Contributors, *Phys. of Plasmas* **14** 055905 (2007).
- [8] C. Angioni and A. G. Peeters, *Phys. Rev. Lett.* **96**, 095003 (2006).
- [9] C. Angioni, R. Dux, E. Fable, A. G. Peeters and the ASDEX Upgrade Team, *Plasma Phys. Control. Fusion*, **49** 2027 (2007).
- [10] H. Nordman, R. Singh, T. Fülöp, L.-G. Eriksson, R. Dumont, J. Anderson, P. Kaw, P. Strand, M. Tokar, and J. Weiland, *Phys. Plasmas*, **15** 042316 (2008).
- [11] T. Fülöp and S. Moradi, *Phys. Plasmas*, **18** 030703 (2011).
- [12] J. Candy, R. E. Waltz, *J. Comput. Phys.*, **186** 545 (2003).
- [13] L. C. Ingesson, H. Chen, P. Helander and M. J. Mantsinen, *Plasma Phys. Contr ol. Fusion*, **42** 161 (2000).
- [14] K. D. Marr, B. Lipschultz, P. J. Catto, R. M. McDermott, M. L. Reinke, A. N. Simakov, *Plasma Phys. and Control. Fusion*, **52** 055010 (2010).
- [15] I. Condrea, E. Haddad, C. Cote and B. C. Gregory, *Plasma Phys. Control. Fusion* **43**, 71 (2001).
- [16] J. E. Rice, J. L. Terry, E. S. Marmor, F. Bombarda, *Nucl. Fusion*, **37** 241 (1997).
- [17] M. Romanelli and M. Ottaviani, *Plasma Phys. Control. Fusion*, **40** 1767 (1998).
- [18] T. Sunn Pedersen, R. S. Granetz, E. S. Marmor, D. Mossessian, J. W. Hughes, I. H. Hutchinson, J. Terry, J. E. Rice, *Phys. of Plasmas*, **9** 4188 (2002).
- [19] J. Carlsson, T. Hellsten, and L.-G. Eriksson. “FIDO, a code for computing the resonant-ion distribution function during ICRH”, Technical Report ALF-1996-104, Alfvén Laboratory, Royal Institute of Technology, SWEDEN, (1996).
- [20] P. Helander, *Phys. of Plasmas*, **5** 3999 (1998).
- [21] T. Fülöp, P. Helander, *Phys. of Plasmas*, **6** 3066 (1999).

- [22] T. Fülöp, P. Helander, *Phys. of Plasmas*, **8** 3305 (2001).
- [23] M. Landreman, T. Fülöp, D. Guszejnov, <http://arxiv.org/abs/1104.0597v1>, submitted to *Phys. of Plasmas* (2011).
- [24] F. Romanelli and S. Briguglio, *Phys. Fluids B*, **2** 754 (1990).
- [25] I. Pusztai, T. Fülöp, J. Candy and J. R. Hastie, *Phys. Plasmas*, **16**, 072305 (2009).
- [26] T. Fülöp and H. Nordman, *Phys. Plasmas* **16**, 032306 (2009).
- [27] C. Angioni, A. G. Peeters, G. Pereverzev, A. Bottino, J. Candy, R. Dux, E. Fable, T. Hein and R. E. Waltz, *Nucl. Fusion* **49** 055013 (2009).
- [28] M. E. Puiatti, M. Mattioli, G. Telesca, M. Valisa, I. Coffey, P. Dumortier, C. Giroud, L. C. Ingesson, K. D. Lawson, G. Maddison, A. M. Messiaen, P. Monier-Garbet, A. Murari, M. F. F. Nave, J. Ongena, J. Rapp, J. Strachan, B. Unterberg, M. von Hellermann and contributors to the EFDA-JET Workprogramme, *Plasma Phys. Control. Fusion*, **44** 1863 (2002).
- [29] M.F.F. Nave, J. Rapp, T. Bolzonella, R. Dux, M.J. Mantsinen, R. Budny, P. Dumortier, M. von Hellermann, S. Jachmich, H.R. Koslowski, G. Maddison, A. Messiaen, P. Monier-Garbet, J. Ongena, M.E. Puiatti, J. Strachan, G. Telesca, B. Unterberg, M. Valisa, P. de Vries and contributors to the JET-EFDA Workprogramme, *Nucl. Fusion*, **43** 1204 (2003).
- [30] O. Gruber, A. C. C. Sips, R. Dux, T. Eich, J. C. Fuchs, A. Herrmann, A. Kallenbach, C. F. Maggi, R. Neu, T. Pütterich, J. Schweinzer, J. Stober and the ASDEX Upgrade team, *Nucl. Fusion* **49**, 115014 (2009).